Friction **11**(1): 93–108 (2023)
https://doi.org/10.1007/s40544-021-0579-0
ISSN 2223-7690
CN 10-1237/TH
RESEARCH ARTICLE

Mechanic model of water-based boundary lubricated contact based on surface force effects

Yanfei FANG[1], **Liran MA**[2,*]

[1] *College of Mechanical Engineering and Automation, Huaqiao University, Xiamen 361021, China*

[2] *State Key Laboratory of Tribology, Tsinghua University, Beijing 100084, China*

Received: 27 July 2021 / Revised: 18 September 2021 / Accepted: 01 December 2021

Abstract: In water-based boundary lubrication regime, the contact gaps (or boundary lubricated film thickness) and surface pressure distribution must be determined to really understand the boundary lubricated contact mechanism. However, the accurate determination of these parameters is limited. In this study, a mechanical model based on boundary lubricated contact involving surface force effects is developed. The surface force distribution characteristics, normal force vs. central film thickness curve, and macroscale water-based boundary lubricated contact are investigated numerically. The results show that hydration directly affects surface force interaction. The accurate boundary lubricated film thickness and surface pressure distribution can be obtained using this model in point contact. Furthermore, the mechanism of macroscale water-based liquid boundary lubricated contact is investigated, in which a water-based boundary lubricated film is formed under appropriate operating conditions based on surface force effects during running-in. This study can reveal the water-base boundary lubricated contact behavior and the carrying capacity of the surface force effect, and provides important design guidance for the surface force effect to achieve liquid superlubricity in water-based boundary lubricated contacts.

Keywords: boundary lubricated contact; surface force; contact behavior; roughness surface; numerical model

1 Introduction

Because water-based lubricants offer advantages of green environmental protection, low cost, and biocompatibility, they are widely used in engineering applications such as bioengineering [1, 2], marine equipment [3], and ceramic bearings [4]. Water-based liquid lubrication yields excellent lubrication performance and has therefore garnered the attention of researchers [5]. Since the water molecular can easily adsorb on the hydrophilic or electrically charged solid surface forming an ordered water layer, the properties of water boundary film exhibit different from the bulk properties of water liquid in boundary lubrication regime [6, 7]. Therefore, the solid–liquid interface effects are vital to the performance of water-based lubrication [8], which is an important research content in water-based boundary lubrication.

In water-based boundary lubrication, owing to the polarity of water molecules and the ionization of ions in aqueous solutions, an electric double layer effect is formed between ions and water molecules on the charged solid–liquid surface under a nanometer-scale gap. The Derjaguin–Landau–Verwey–Overbeek (DLVO) theory can be used to describe the electric double layer (EDL) and van der Waals interactions between two planar surfaces in thin liquid film. The interaction distance of the electric double layer is relatively long, and the kinetic electric viscosity generated during motion affects the rheology of the water-based lubricant under the nano thin film [9]. Some researchers discovered that the effect of the electric double layer is vital to water-based nano thin film lubrication under macroscale motions from experiment and numerical approach [10–15]. While the surface contact gap is down into the molecular scale, researchers have

* Corresponding author: Liran MA, E-mail: maliran@tsinghua.edu.cn

Nomenclature

a	Hertz contact radius, m	rms	root mean square of surface height, m
a_w	Radius of the ball wear surface, m	R	Equivalent radius of ball, m
A_H	Hamaker constant, J	R_e	Equivalent radius of surface after running-in, m
E	Effective elastic modulus, GPa	T	Absolute temperature, K
F	Normal load, N	x, y, z	Position coordinates
h	Contact gaps or boundary film thickness, m	β_x, β_y	Autocorrelation lengths of the surface profile along the x-axis, y-axis direction, m
h_0	Original gap between ball and disc, m	γ	Surface energy, J
h_w	Ball geometric shape, m	γ_c	Proportion of the load supported by the asperity contact in the total load, %
k	Boltzmann constant	δ	the comprehensive surface roughness height, m
l_0	Equilibrium separation, m	ε	Parameter determining the depth of the potential well, J
p_c	Asperity contact pressure, Pa	κ	Debye length, m
p_{EDL}	Electric double layer acting pressure, Pa	λ	Hydration decay constant, m
p_H	Maximum Hertz contact pressure, Pa	σ	Distance at which the interparticle potential is zero, m
p_{hyd}	Hydration acting pressure, Pa	φ	Surface potential, V
p_{hyd0}	Hydration constant of different lubricant, Pa		
p_{vdW}	van der Waals attraction pressure, Pa		
p_s	Surface pressure, Pa		
p_{rep}	Short-range repulsive contact pressure, Pa		

found hydration interactions under this nanoconfined condition [16–18]. Water molecules are firmly adsorbed onto the interface to form an interface hydration layer on a hydrophilic surface. When the surfaces adsorb the hydration layer, they can provide a high pressure to support an external load [18, 19]. Based on the surface force appearance, Ma et al. [20] analyzed the surface force action and friction dissipation form of a NaCl water solution. Diao and Espinosa-Marzal [21] performed atomic force microscopy (AFM) test to measure and analyze the DLVO and hydration effect considering calcite's nonclassical Stern layer on nanoconfined calcite–solution interface. These studies confirmed that surface forces varied from long-range van der Waals attraction and electric double layer forces to short-range strong hydration forces, thereby affecting the boundary lubrication contact behavior in electrolyte solutions. Li et al. [22] investigated the lubrication contact characteristics between silica spheres and substrates of different wettability in an aqueous solution. The surface force was primarily the competition between van der Waals attraction and repulsive hydration interaction. In these studies, investigations were primarily based on experiments to explore the mechanic of the water-based boundary lubricated contact behavior considering surface force effects. However, the quantitative determination of macroscale boundary lubricated contact behavior such as the contact gaps (or boundary film thickness) and surface pressure distribution based on surface forces remains challenging.

Meanwhile, the shear force between the water molecular layers becomes extremely weak to achieve excellent lubrication. In water-based liquid lubricated contact, different surface force interactions directly affect the macroscale contact behavior, sometime benefitting for achieving ultralow friction lubrication. Therefore, water-based liquid superlubricity systems have garnered considerable attention [23, 24]. Based on experiments, researchers discovered that a boundary thin film was present when superlubricity is reached as water molecules adsorbed on the two friction surfaces under water-based liquid lubricated point contact after running-in [25, 26]. During running-in of steel/steel friction pairs sliding contact, Ge et al. [27] pointed out that the tribochemical layers, ordered layers, and

a fluid layer were formed during the superlubricity periods. The relatively soft tribochemical layer helps to reduce the contact pressure after running-in, which attributing to reduce the friction coefficient. Moreover, the interface adsorption can form an ordered lubricated film with molecular orientation on the solid–liquid interface. Liang et al. [28] discovered that the lubrication state may transit into thin film lubrication at high speeds under severe starvation. They thought that the possible mechanism is that the high-speed flow prompts the rearrangement of lubricant molecules at the interface to form an ordered lubricating film. Relevant experiments confirmed this hypothesized mechanism of orderly arrangement lubricant that enhances the film-forming ability and reduces the friction coefficient [29]. So, it can be summarized that the ordered layers on interface enhances the surface force effects, which provide strong carrying capacity to benefit for the realization of ultralow friction under boundary lubrication. Han et al. [30, 31] proved that macroscale liquid superlubricity of point contact can be realized through the boundary hydration effect generated in different salt ion solutions after running-in. Li et al. [32] introduced hydrated salt ions into a polymerized aqueous solution to achieve liquid superlubricity under a high pressure via the synergistic effect of the hydrodynamic effect and boundary hydration effect. Although great progress has been made in the study of water-base boundary lubrication with ultra-low friction based on surface force by experiment approach, there are still some shortcomings in the analysis of numerical theoretical model. A few researchers [15, 33, 34] analyzed the contribution of surface force effects to thin film lubrication based on the modified Reynolds equation coupling surface force action to investigate ultralow friction liquid lubrication. However, the quantitative analysis of the carrying capacity of the surface force effects to achieve liquid superlubricity is less studied. To bridge this gap between experiment and theoretical model, this study attempts to propose a numerical model of water-based boundary lubrication based on surface force effects in point contact, to investigate the mechanism of water-based liquid superlubricity, especially the hydration force effect.

Herein, a universal equation for surface force interaction is proposed for a water-based boundary lubrication contact problem. Subsequently, a macroscale water-based boundary lubrication model based on the surface force effects is established in point contact. Then, the numerical calculation procedure for this model is provided. Finally, the effect of hydration on the surface force distribution, the characteristic curves of normal load vs. central film thickness, and the macroscale boundary lubricated contact behavior based on surface force in roughness surface point contact are analyzed. This mechanical model can provide insights into the macroscopic water-based boundary lubricated contact behaviors with the molecular interaction at the nanoscale. Furthermore, the mechanics of water-based liquid boundary lubricated contact behavior is revealed, which can provide an effective numerical analysis method and theoretical guidance for water-based boundary lubrication performance.

2 Boundary lubricated contact model based on surface force effects

2.1 Surface force effects

The charged solid surface can selectively adsorb ions with opposite charges in the polar solution, most notably ions in water. Ions with the same charge are repelled from the outer layer, thereby yielding charge balance and forming electric double layer electrostatic interactions at the solid–liquid interface. According to electrostatic interaction theory, the pressure exerting on an electric double layer can be expressed as Eq. (1) [8]:

$$p_{\mathrm{EDL}}(x,y)=p_{\mathrm{EDL0}}\tan h^2(ze\varphi/4kT)\mathrm{e}^{-\kappa h(x,y)} \quad (1)$$

where $p_{\mathrm{EDL0}}=64kT\rho_\infty$, k is the Boltzmann constant, T is the absolute temperature, ρ_∞ is the molecular number density, Z is the valency of the ion, e is the number of charges (1.602×10^{-19} C), φ is the surface potential (V), κ is the Debye parameter, and $h(x,y)$ is the contact gap or boundary film thickness.

As contact gap decreases down molecular scale, water molecules are tightly bound to ions or ionized surfaces in an aqueous medium, thereby resulting in the formation of a hydration layer on the solid–liquid interface. The effect of the hydration layer can generate a high repulsion pressure when the two

surfaces are in the subnanometer scale (approximately 1 nm distance). Several researchers have proposed an average exponential function to represent the interfacial hydration pressure action, as Eq. (2) [16, 17]:

$$p_{\mathrm{hyd}}(x,y)=p_{\mathrm{hyd0}}\mathrm{e}^{-h(x,y)/\lambda_0} \tag{2}$$

where p_{hyd0} is the hydration constant and λ_0 is the hydration decay constant. Through Eqs. (1) and (2), both the electric double layer and hydration forces decay based on an exponential function, and their most influencing factor is their interaction distance.

Meanwhile, the solid surface exhibits a van der Waals attraction force and a short-range repulsive contact force. The van der Waals attraction force originates from the material's inherent polarization, whereas the repulsive contact force originates from the overlapping of electron clouds when the molecular spacing is small. These two forces generally appear in the interaction contact surface region. In general, the Lennard–Jones (L–J) potential energy between two atoms can be expressed as

$$w(h(x,y))=4\varepsilon\left[\left(\frac{\sigma}{h(x,y)}\right)^{12}-\left(\frac{\sigma}{h(x,y)}\right)^{6}\right] \tag{3}$$

where ε is the depth of the potential well, and σ is the distance at which the interparticle potential is zero.

The potential energy of the L–J surface action can be used to deduce the van der Waals attraction and repulsive pressure at any point on the surface [35, 36]. Hence, the formula for the van der Waals attraction pressure can be obtained as Eq. (4):

$$p_{\mathrm{vdW}}(x,y)=-\frac{A_{\mathrm{H}}}{6\pi l_0^3}\left(\frac{l_0}{h(x,y)}\right)^3 \tag{4}$$

The short-range repulsive pressure is expressed as

$$p_{\mathrm{rep}}(x,y)=\frac{A_{\mathrm{H}}}{6\pi l_0^3}\left(\frac{l_0}{h(x,y)}\right)^9 \tag{5}$$

where A_{H} is the Hamaker constant and l_0 is the equilibrium distance between the surfaces. According to Ref. [36], Eqs. (4) and (5) can also be described via the surface adsorption energy, which can be characterized by the surface wettability, which is expressed as

$$p_{\mathrm{vdW}}(x,y)=-\frac{8\Delta\gamma}{3l_0}\left(\frac{l_0}{h(x,y)}\right)^3 \tag{6}$$

$$p_{\mathrm{rep}}(x,y)=\frac{8\Delta\gamma}{3l_0}\left(\frac{l_0}{h(x,y)}\right)^9 \tag{7}$$

Here, $\Delta\gamma$ is the energy of adhesion expressed as $\Delta\gamma=\gamma_1+\gamma_2-\gamma_{12}$ and γ_1, γ_2, γ_{12} are the surface energies of the two bodies and their interface, respectively. Surface wettability can be changed by modifying the physical and chemical properties of the surface.

Figure 1 shows an illustration of the interaction surface force between two surfaces under an aqueous lubricated point contact. In this study, the water-based solid–liquid surface force effects are primarily considered, including the hydration force, electric double layer effect, van der Waals attraction force, and repulsive contact force between the contact surfaces. Those surface forces have their interaction distance. The van der Walls attraction with weak interaction usually exists between any two surfaces. With the separation gap decreased, the EDL and hydration force play a leading role since they have different characteristic distance, respectively. Hydration has shorter interaction length than the EDL interaction. Once liquid molecules are squeezed out, the solid atoms are directly contact caused by the short-range solid repulsive. Under this condition, it could be

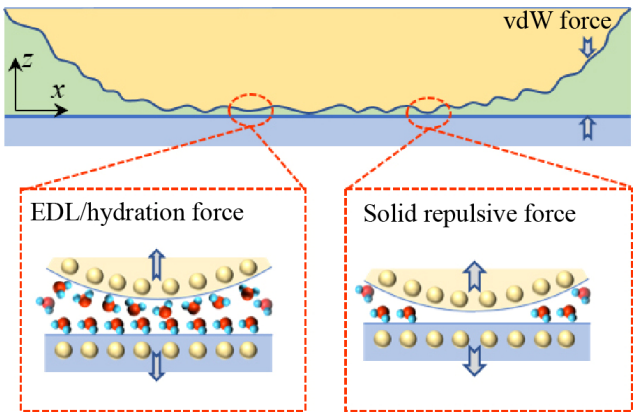

Fig. 1 Schematic illustration of interaction surface force under aqueous lubricated point contact.

considered that the contact would be degraded to the normal rough surface contact model. Therefore, it can be assumed that their interactions are independent of each other, they can be added to each interaction distance. The surface pressure can be expressed as

$$p_s(x,y)=p_{hyd}(x,y)+p_{EDL}(x,y)+p_{vdW}(x,y)+p_{rep}(x,y) \quad (8)$$

The distribution of the surface force is determined based on the physical and chemical characteristics of the contact surface and boundary lubricant molecular structure. For different situations, if only the surface adhesion contact is considered, then the surface pressure is composed of the van der Waals force and short-range repulsive force based on the L–J potential. Subsequently, Eq. (8) can be simplified expressed as

$$p_s(x,y)=p_{vdW}(x,y)+p_{rep}(x,y) \quad (9)$$

In the microscopic interaction between colloids or nanoparticles, the interaction force between two surfaces is primarily comprised of the van der Waals attraction and electric double layer interactions, which is the classic DLVO theory. Hence, Eq. (8) can be written as

$$p_s(x,y)=p_{vdW}(x,y)+p_{EDL}(x,y) \quad (10)$$

By compared between Eqs. (9) and (10), it can be inferred that Eq. (8) is more universal for describing the surface force interaction and can account for a wider range between the contact surfaces.

2.2 Boundary lubricated point contact

In the macroscale contact profile between the worn ball and plane substrate, as shown in Fig. 2, it can be equivalent to the contact between the elastic ball and rigid plane. The surface contact gap is also defined as the boundary lubricated film thickness between the contact surfaces. The boundary film thickness can be expressed as

$$h(x,y)=h_0+h_w(x,y)+u(x,y)+\delta \quad (11)$$

where h_0 is the rigid gap, $h_w(x,y)$ is the spherical geometric profile shape considering that the surface contact profiles can be changed after running-in, δ is the comprehensive surface roughness of the contact surface, and $u(x,y)$ is the surface elastic normal deformation. The composite elastic normal deformation of the two surfaces $u(x,y)$ due to surface pressure $p_s(x,y)$ over the region Ω_c can be determined by the Boussinesq integral formula is expressed as

$$u(x,y)=\frac{2}{\pi E}\iint_{\Omega_c}\frac{p_s(x',y')}{\sqrt{(x-x')^2+(y-y')^2}}\mathrm{d}x'\mathrm{d}y' \quad (12)$$

where E is the effective elastic modulus of two contact homogeneous material.

Owing to the running-in wear under the ball–disk sliding contact, the geometric shape of the spherical surface will be changed, as shown in Fig. 2. Based on the contact geometry after running-in wear and the Hertz contact theory, the following geometry equations

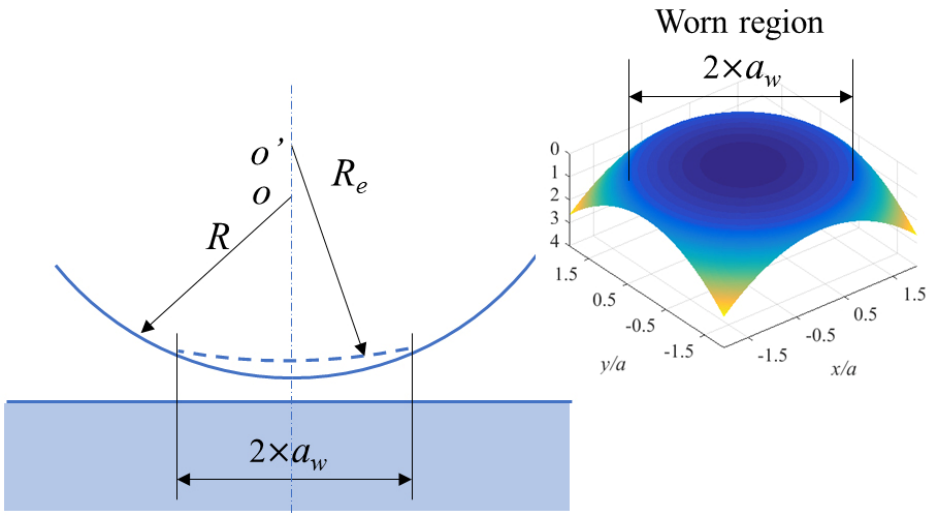

Fig. 2 Contact profile geometry considered during running-in.

are proposed:

$$h_w(x,y)=\begin{cases} R-\sqrt{R^2-(x^2+y^2)} & x^2+y^2 \geq {a_w}^2 \\ R_e-\sqrt{R_e^2-(x^2+y^2)}+h_e & x^2+y^2 < {a_w}^2 \end{cases} \tag{13}$$

where R is the radius of the ball, R_e is the curvature radius of the worn spherical surface, h_e is determined by the geometric relationship: $h_e=\sqrt{{R_e}^2-{a_w}^2}-\sqrt{R^2-{a_w}^2}+R-R_e$, and a_w is the radius of circular worn region on the ball surface and a_w should be greater than or equal to the Hertz contact radius a. According to the Hertz contact theory, the equivalent radius of the surface after running-in can be obtained: $R_e=\dfrac{2{a_w}^3E}{3F}$.

Because the applied load F is constant, the balance equation of the contact surface pressure and load can be determined as Eq. (14):

$$F=\iint p_s(x,y)\mathrm{d}x\mathrm{d}y \tag{14}$$

Based on Eqs. (8), (11), and (14), the established numerical model can be considered as a combination of the microscopic effect of lubricant molecules on the lubricated surfaces and the macroscale point contact between two surfaces with water-based lubricant. This numerical model can be extended to obtain the boundary lubricated film thickness and surface pressure under different conditions, such as oil-based lubricant.

2.3 Numerical calculation process

To facilitate the calculation process, the main control equations are first normalized. The following dimensionless parameters are defined: $X=\dfrac{x}{a}$, $Y=\dfrac{y}{a}$, $H=\dfrac{hR}{a^2}$, and $P_s=\dfrac{p_s}{p_H}$ (considering the macroscale contact analysis), where a is the Hertz contact radius and p_H is the maximum Hertz contact pressure in point contact. The calculation region is determined based on the operating conditions, and the grid nodes are partitioned into 256 × 256 square elements. Using these dimensionless parameters, all equations of the surface acting pressure, lubricated contact gap, and load balance are deduced as dimensionless equations. Finally, the dimensionless equations are discretized for the numerical calculation.

The programming calculation for this model is performed in MATLAB. In the calculation, the initial value of the contact pressure directly impacts the convergence of the calculation and the improper initial value could lead to the failure of the calculation. Hence, based on the contact surface profile, the conjugate gradient method (CGM) and discrete convolution–fast Fourier transform (DC–FFT) method are adopted to solve the elastic contact problem to obtain the initial surface pressure [37, 38]. The calculation has been proven to be convergent for smooth and rough surface contact problem solution. The contact pressures obtained via the CGM and DC–FFT are applied as the initial surface pressures. After that it enters the iterative calculation, the elastic deformation is calculated by means of DC–FFT method and contact gap (boundary film thickness) could been then obtained. Subsequently, Using the surface force equation to get the new surface pressure, a relaxation iteration method is used to determine final surface pressure. Then, check whether convergence conditions of load balance and surface pressure are satisfied. In the calculation, the load balance and pressure convergence conditions are both set as $\dfrac{|W-F|}{F}\leq 1.0\times10^{-3}$ and $\dfrac{\sum_{i=1}^{Nx}\sum_{j=1}^{Ny}|p_{ij}^{k+1}-p_{ij}^{k}|}{\sum_{i=1}^{Nx}\sum_{j=1}^{Ny}p_{ij}}\leq 1.0\times10^{-3}$, where W is calculated normal load in the each iterative. If the load balance and pressure convergence condition are not satisfied, the calculation enters into the next iteration. The contact gap is adjusted by increasing or decreasing the thickness ΔH. The pressure distribution is re-calculated and then check the convergence conditions again. The calculation is terminated when the convergence conditions are satisfied. The contact gap (boundary lubricated film thickness) and surface pressure distribution under different conditions are output. The flowchart of the proposed numerical solution is shown in Fig. 3.

It is noteworthy that for the calculation, the relaxation factor selection is determined based on

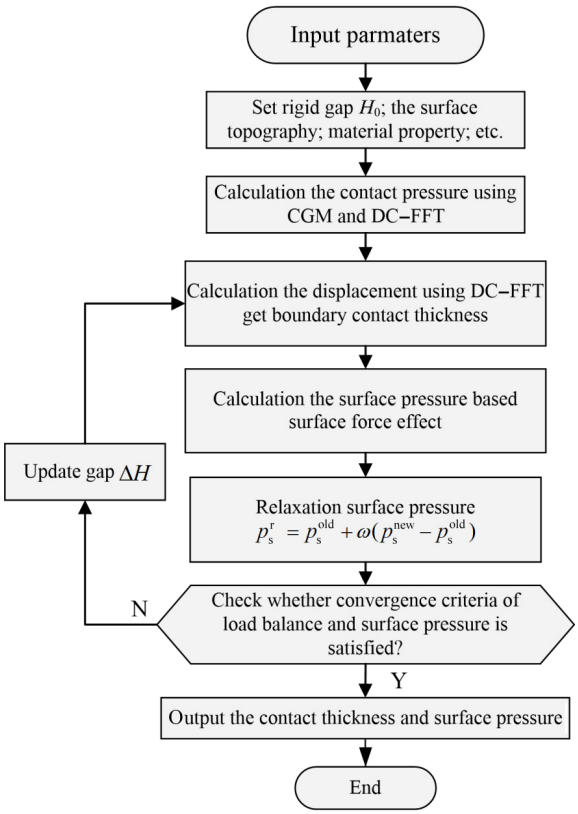

Fig. 3 Flowchart of the numerical calculation for this model.

the operating conditions, which would affect the convergence procedure, particularly when the contact gap is less than the equilibrium distance l_0. Because the contact pressure of the solid surface contact can change significantly under this situation, the calculation will fail to converge. Therefore, a lower relaxation coefficient ranging from 0.01 to 0.0001 is recommended in different cases to ensure calculation convergence.

3 Results and discussion

3.1 Surface force distribution characteristics

Initially, the surface force distribution characteristics are emphasized in the numerical investigation. To select the surface force parameters, the parameters of the electric double layer are set as follows: $p_{EDL0} = 15.9\times10^6$ Pa, Debye length $\kappa^{-1} = 1.36$ nm, electric potential $\varphi = 70$ mV, and Hamaker constant $A_H = -2\times10^{-20}$ J; meanwhile, the equilibrium distance of the solid surface is set as $l_0 = 0.2$ nm. These parameters will be used in all examples discussed below. The hydration force parameter is set as $p_{hyd0} = 1.00\times10^9 - 0.10\times10^9$ Pa, and the decay length of hydration is changed from 0.2 to 0.5 nm. All those parameters are cited from the Refs. [8, 20]. Figure 4 shows the curve distribution of different interaction pressures and distances. Figure 4(a) shows the surface force distribution under the action of the L–J potential energy, i.e., the classical surface adhesion interaction pressure distribution. The contact behavior can be analyzed based on adhesion contact [39, 40]. For water-based lubricated contact, the form of surface force effect function is shown in Eq. (8), and the curves shown in Figs. 4(b) and 4(c) can be obtained by substituting parameter values.

Figure 4(b) shows the curve of interaction pressure vs. separation distance for various values of hydration capacity, and the hydration decay length is 0.2 nm. Under a large gap (≥ 2 nm), the water molecules are weakly restricted, and the freedom of the water molecules is high, which decreased the interaction pressure between two surfaces. The surface force is combined with the static electric double layer and the van der Waals effect as the royal blue dash line shown in Fig. 4(b). It can be discovered that the electric double layer interaction distance is relatively large, but its interaction ability is inferior relative to the hydration effect. As the contact distance is decreased from 2.0 to 0.4 nm, the surface interaction pressure range is increased from several megapascal to hundreds of megapascal as the purple dash line shown in Fig. 4(b). The hydration interaction plays a dominant role that can support high pressure at molecular scale. While the hydration capacity decreased as $p_{hyd0} = 0.10$ GPa, the hydration repulsive pressure is extremely weak, and the maximum pressure is only approximately several megapascal. It can be inferred that under this surface force interaction, the hydration bearing capacity is extremely weak. Meanwhile, considering the same hydration capacity ($p_{hyd0} = 1.00$ GPa), the hydration decay length varied from 0.2 to 0.5 nm. Figure 4(c) shows the interaction pressure vs. separation distance for various hydration decay lengths. As the hydration decay length increased, the distance in which the hydration pressure is exerted increases significantly.

Finally, when the contact gap is less than 0.2 nm, the surface pressure increases significantly, even can exceed several gigapascals. It can be thought that two surfaces are in contact through the surface solid

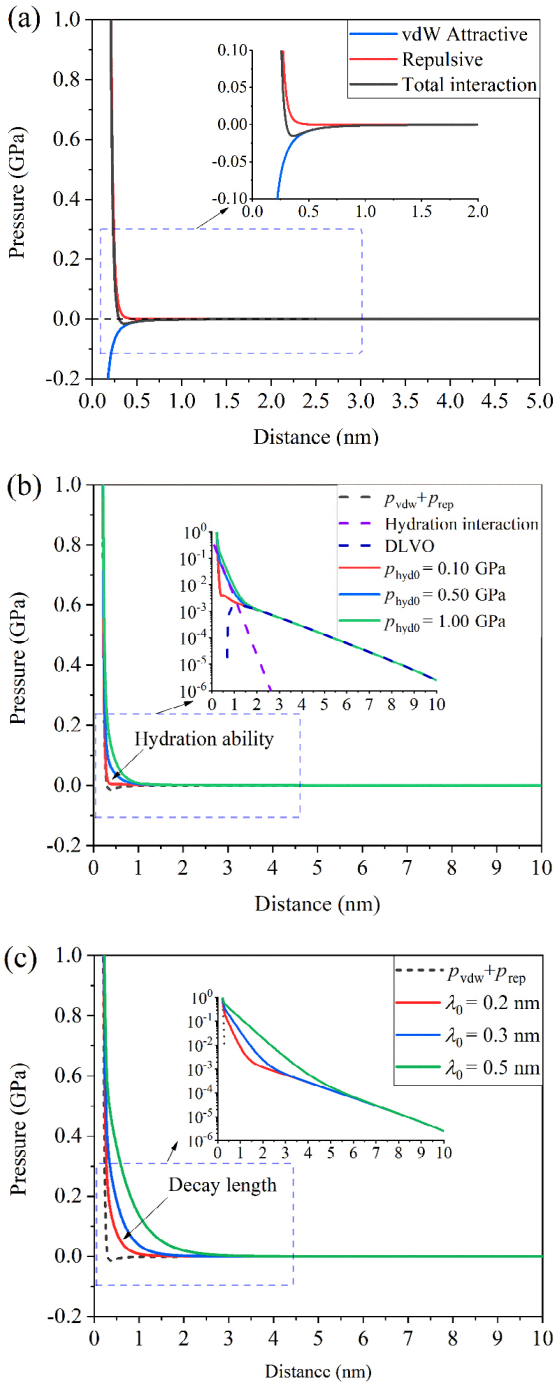

Fig. 4 (a) Interaction pressure vs. distance based on L–J potential, (b) effect of hydration ability on surface interaction pressure distribution (λ_0 = 0.2 nm), and (c) effect of decay length on surface interaction pressure distribution (p_{hyd0} = 1.00 GPa).

asperities under this state, that means it degrades to the normal contact. Based on this analysis, it can be inferred that the proposed Eq. (8) of surface force interaction involves multi surface force effects from solid repulsion, hydration interaction, and the electric double layer to the van der Waals effect. Hence, the analysis provides valuable insights for macroscale contact modeling.

3.2 Boundary lubrication contact behavior under surface force interaction

The surface force apparatus can be applied to measure the surface force interaction between atomically smooth mica surfaces of two crossed cylinders. According to Hertzian mechanics theory, the contact of a sphere ball over an elastic half-space plane with a boundary lubricated film is equivalent to the contact between two crossed cylinders. The proposed model is applied to investigate the contact behavior of the surface interactions. The contact radius is 1 cm, the equivalent elastic modulus is E = 60 GPa, that is determined by using mica as a contact material, and the surface force is set based on the parameters presented in Section 3.1; meanwhile, the hydration effect is set based on p_{hyd0} = 1.00 GPa and λ_0 = 0.2 nm. Subsequently, the boundary lubricated film thickness and surface pressure distribution between two surfaces are calculated.

Figure 5 shows the boundary lubricated film thickness and surface pressure distribution under different loads on the y axis. According to the thickness distribution of the boundary lubrication, both the electric double layer and van der Waals force serve as a primary function of supporting under a relative low normal load. Under this condition, the boundary film is thicker and the contact surface profile is almost not deformed because of the low surface pressure. There is obviously no finite contact radius under low normal load as shown in Fig. 5(a). With the load increases, the boundary film thickness is gradually decreased. Contact surface deformation intensified and the contact region flattened as the increase of surface pressure. the hydration interaction gradually plays contributions to support the normal load. On the other hand, the pressure distribution is relatively wider than that the classical Hertz contact area, and differs from the classical Hertz contact pressure distribution under the low normal load as shown by the dotted line in Fig. 5(b). It can be clearly found that the maximal pressure is smaller than the maximal Hertz contact pressure and the pressure distribution

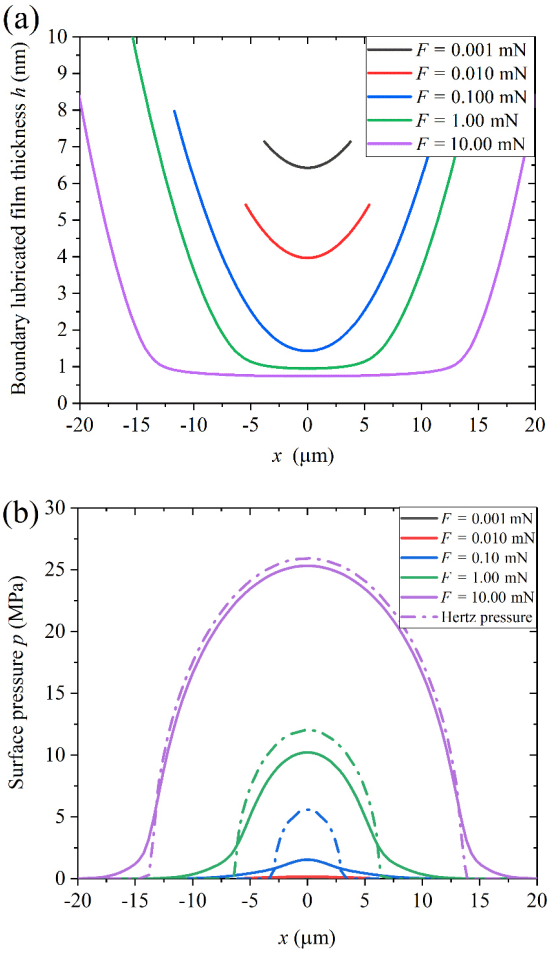

Fig. 5 (a) Boundary lubricated film thickness and (b) surface pressure under different loads.

region is become larger as for the surface force interaction. Once the normal load continues to increase, the boundary lubrication film thickness thins down to approximately 2 nm. Subsequently, the hydration effect becomes particularly important for supporting the applied normal load. When the normal load is 10 mN, the boundary lubricated thickness is mostly less than 1 nm, the surface pressure is almost contributed by hydration interaction. It can also be observed that the hydration pressure distribution of the interface is similar to the pressure distribution of the elastic Hertz point contact under high normal load, and the maximum surface pressure is 25.31 MPa, that is marginally less than the maximal Hertz contact pressure 25.92 MPa.

Figure 6 shows the curve of normal forces vs. the boundary film thickness at the surface center across several aqueous solutions. It is discovered that the

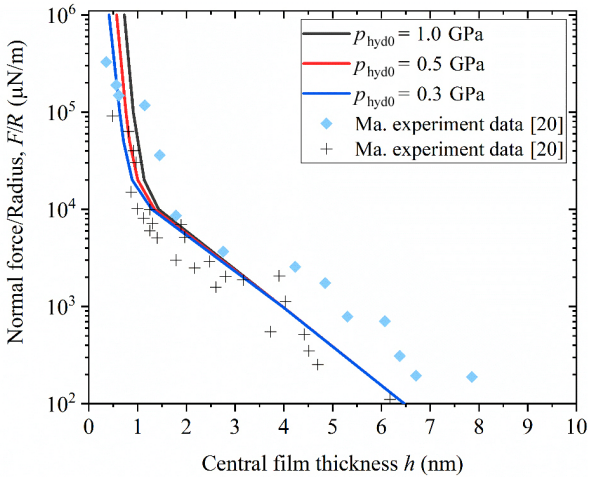

Fig. 6 Curve of applied normal force F/R vs. central film thickness.

normal force vs. film thickness curves calculated using the present method is very similar to the experiment results presented in Ref. [20]. This verifies the validity of the established model and the numerical algorithm. The normal load is supported by the electric double layer and van der Waals effect under the long-range interaction. As the boundary film thickness decreases to 1 nm, the normal bearing capacity increases significantly via the hydration effect. When the hydration constant decreases from 1.0 to 0.3 GPa, it can be inferred that the hydration capacity reduces, and the central film thickness between two surfaces is getting closer under larger normal forces. Therefore, surface modification can be applied to enhance surface hydrophilic adsorption, such as that polymer molecules can be introduced to enhance the capability of surface hydration ability so that the contact film thickness in the contact area can be increased and an effective boundary lubricated layer is formed [41].

These results show that the proposed model can be effectively applied to quantitatively analyze the water-based liquid boundary lubricated contact behavior based on surface force effects. Furthermore, if the surface force interaction can be obtained under oil-based boundary lubrication experimentally, then the Eq. (8) can be modified, and the proposed model can be extended to oil-based boundary lubrication contacts to determine the contact boundary film thickness and pressure accurately, which will be following research work to carry out.

3.3 Macroscale water-based boundary lubricated contact behavior

In this section, macroscale boundary lubricated contacts based on the surface force effect are analyzed. Furthermore, the ultralow friction lubrication state is explained based on hydration lubrication. The input parameters in this example are that: An applied load is 3 N, the comprehensive elastic modulus is set as 250 GPa, and the sphere radius is 2 and 8 mm, respectively. The surface force action parameters are set based on Section 3.2. To quantitatively analyze the contact load capacity, the load-bearing ratio is defined as $\gamma_c = \dfrac{\iint_{\Omega_c} p_c(x,y)\mathrm{d}x\mathrm{d}y}{F}$, which reflects the proportion of the load supported by the asperity contact in the total load. When the contact gap is less than 0.2 nm, it is considered as the rough asperities contact between solid surfaces, that p_c is defined as asperity contact pressure.

The rough surface topography is assumed to be a Gaussian height distribution, which is generated by two-dimensional digital filtering technology [42], as shown in Fig. 7. Readers are referred to Ref. [42] for further details. The root mean square of surface heights (rms) is changed from 3 to 9 nm. Subsequently, the surface roughness height data can be used in Eq. (11) to consider the effect of roughness on the contact behavior.

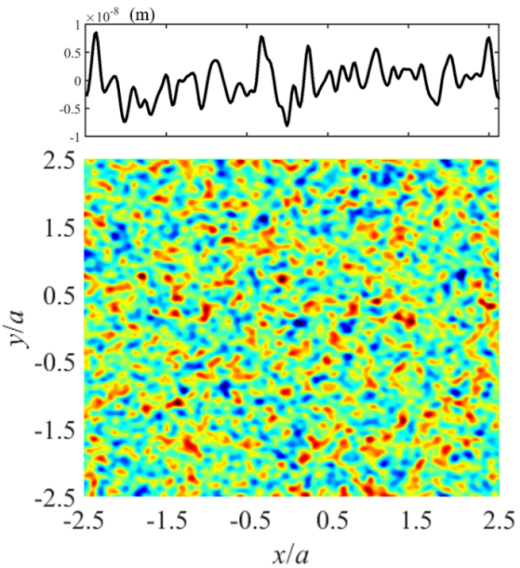

Fig. 7 Gaussian random rough surface generation (rms = 3 nm, $\beta_x = \beta_y = 1/64\,a$).

Figure 8 shows the distribution of the boundary lubricated contact film thickness and pressure before and after running-in based on the cross section of y = 0 for a sphere radius of 2 mm (F = 3 N, E = 250 GPa, and rms = 3 nm). The Hertz contact radius is a = 33.02 μm, and the maximum pressure can reach p_H = 1.31 GPa. The radius of circular worn region on the ball a_w is 1.60a = 52.83 μm after running-in. It is observed that the minimum contact gap in the whole region is 0.15 nm, and the rough asperities in the contact area flattened under high pressure before running-in. The applied load is supported by the atoms between the solid surfaces in the contact area. As the running-in wear area increases, the pressure in the contact area decreases significantly, but the pressure in the contact area is primarily borne by the rough peak and hydration pressure. It can be determined via calculation that the load bearing ratio

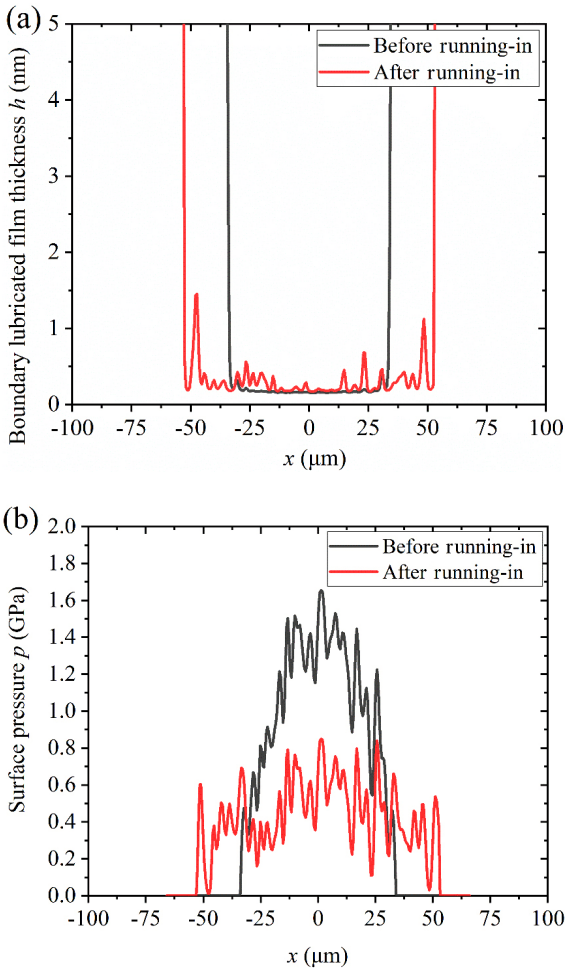

Fig. 8 (a) Boundary lubricated film thickness and (b) surface pressure before and after running-in (R = 2 mm).

of the asperity contact before running-in is $\gamma_c = 92.6\%$, whereas the load bearing ratio of the asperity contact after running-in is $\gamma_c = 34.8\%$. Under this condition, the contact pressures of the rough peak still exist and support the normal load partially. It is speculated that the friction force in the lubricated contact area will be reduced after running-in, but it remains relatively high.

Figure 9 shows the distribution of the boundary lubricated contact film thickness and pressure before and after running-in based on the cross section of y = 0 for a sphere radius of 8 mm (F = 3 N, E = 250 GPa, and rms = 3 nm). According to the Hertz contact theory, it is calculated that the Hertz contact region radius a is 52.42 μm, and the maximum contact pressure p_H is 521.38 MPa. Before running-in, owing to the rough peak, the contact pressure exceeds 600 MPa, and the gap at the center of the contact area

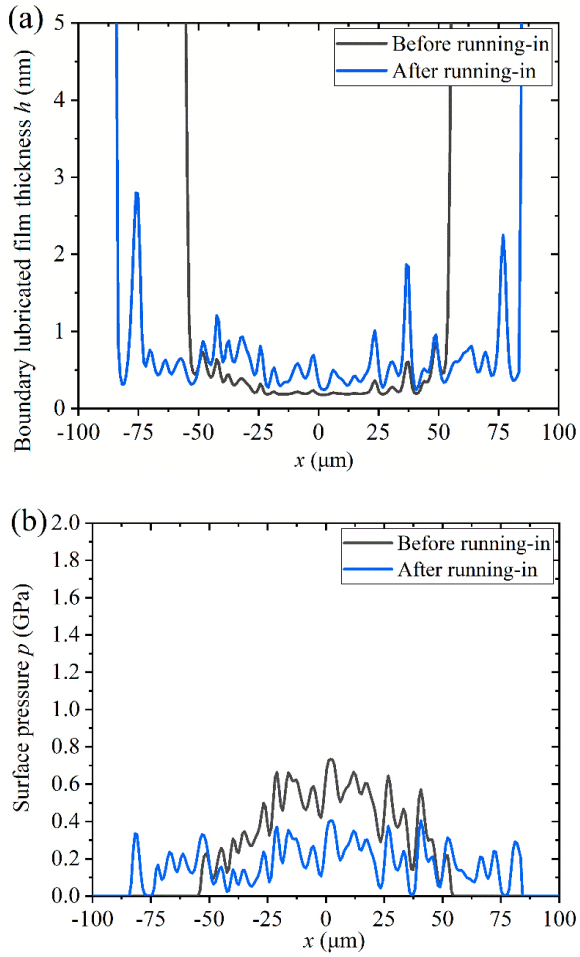

Fig. 9 (a) Boundary lubricated film thickness and (b) surface pressure before and after running-in (R = 8 mm).

is 0.17 nm. The abovementioned pressure can be regarded as the solid atom repulsive contact pressure, and hydration boundary lubrication could not be formed. After running-in is performed, the radius of circular worn region on the ball a_w is set 1.60a = 83.86 μm, the average pressure is approximately 100 MPa, and the gap in the contact center area exceeds 0.30 nm; this implies that a few solid rough peak contacts appeared. By comparing the load-bearing ratios of $\gamma_c = 24.7\%$ and $\gamma_c = 0.4\%$ before and after running-in, respectively, it can be discovered that the hydrated film on the boundary lubrication area is formed at this condition. In this state, it is beneficial to realize an ultralow friction coefficient of hydration boundary lubrication.

During running-in, the newly generated surface roughness affects the lubricated-boundary contact behavior. The calculation parameters are as follows: Ball radius of 8 mm, applied load of 3 N, elastic modulus of 250 GPa, and the radius of circular worn region on the ball after running-in a_w = 83.86 μm. The surface roughness rms is set as 3, 6, and 9 nm, respectively. Figure 10 shows the effect of surface roughness on the boundary lubricated film thickness and surface pressure distribution on the y axis. The increasing of roughness resulted in more asperity contacts, and surface contact pressure is increased. Figure 11 shows boundary lubricated film thickness and surface pressure distribution for rough ball of different roughness in the contact region. it can be also easily found that the surface force effect can be reduced with the roughness increased. It can be calculated that the load-bearing ratio γ_c of the asperity contact increased from 0.4% to 14.3% to 37.7% with the roughness rms increased. In other words, the lubricated film thickness can increase with the roughness rms decreased. Therefore, it can be inferred that during running-in, the surface roughness directly affects the boundary lubricated contact behavior. The newly generated surface roughness is expected to be effectively reduced during running-in such that a hydration layer can be formed to support the load.

Furthermore, as a tribomechanical chemical reaction occurs during running-in, particularly in ceramic materials, a new reaction film is generated in the contact region. Consequently, the mechanical properties

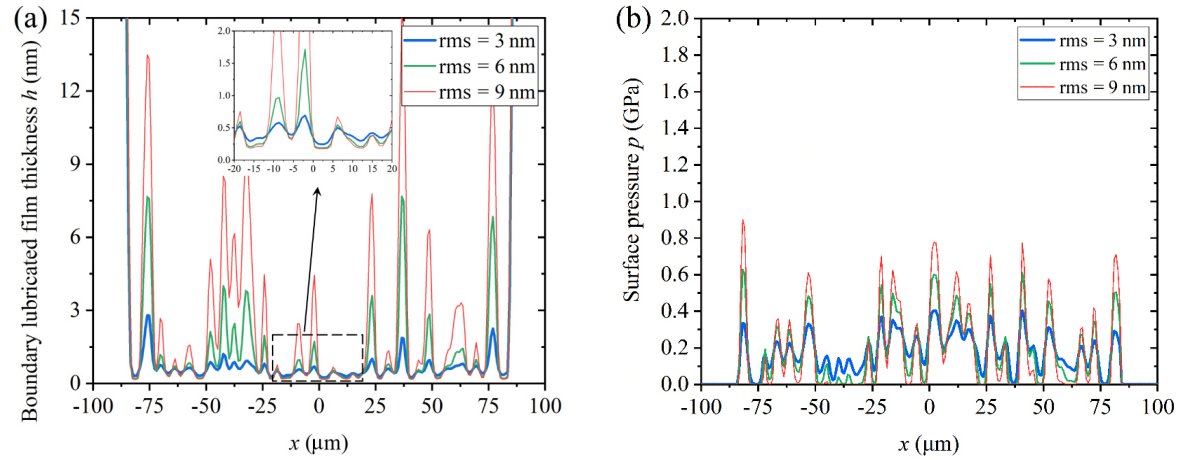

Fig. 10 Effect of surface roughness on (a) lubricated-boundary film thickness and (b) surface pressure.

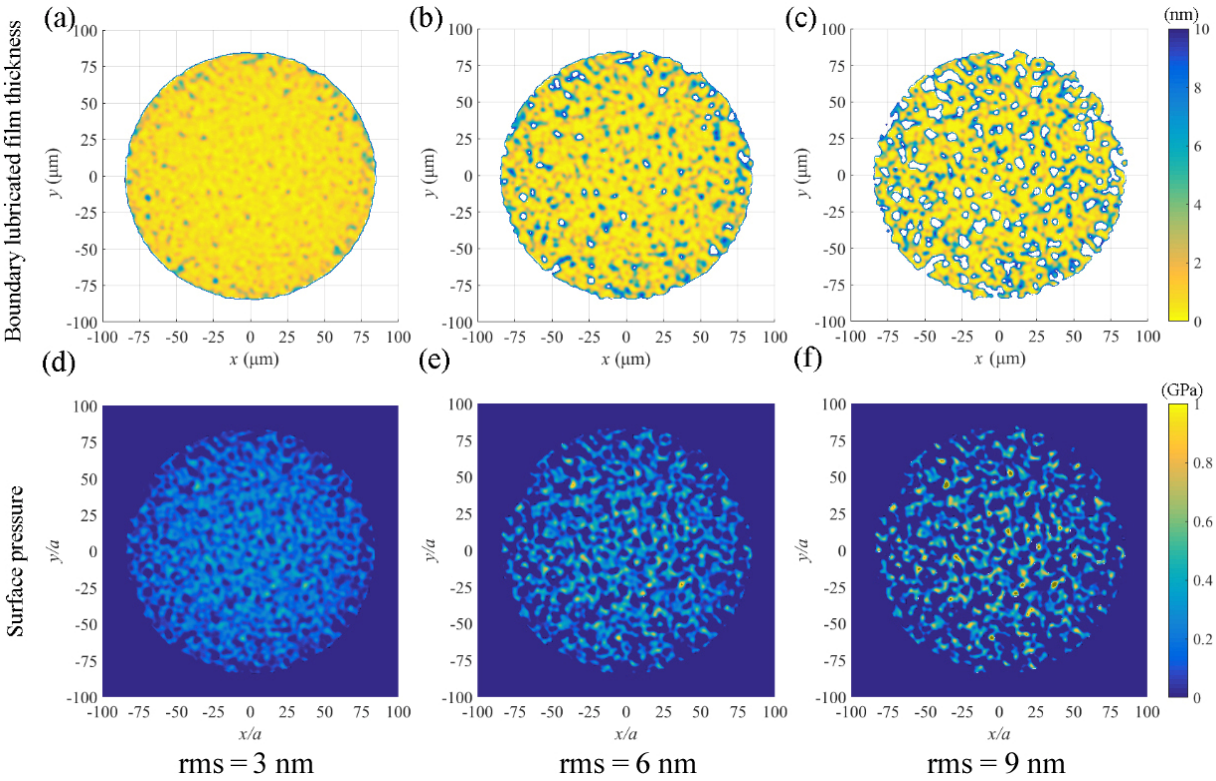

Fig. 11 Surface pressure and lubricated-boundary film thickness for rough ball of different roughness.

of the reaction film can be changed. In this part, the effect of the elastic modulus of the contact material on the boundary-lubricated contact behavior is investigated. The effective elastic modulus of contact system E is set as 250, 175, and 100 GPa (F = 3 N, rms = 3 nm, R = 8 mm), respectively. It can be calculated that Hertz contact radius a is 52.415, 59.03, and 71.11 μm, correspondingly. All of the radius of circular worn region on the ball after running-in a_w are set the same value as 83.86 μm. Figure 12 shows the effect of effective elastic modulus on the boundary lubricated film thickness and pressure distribution on the y axis. It can be observed that the effective elastic modulus of the contact pair reduced, resulting in a reduced contact pressure. As the boundary lubricated film thickness increased, the surface force effect resulted in the formation of an effective boundary lubricated film. It is beneficial to improve the lubrication performance

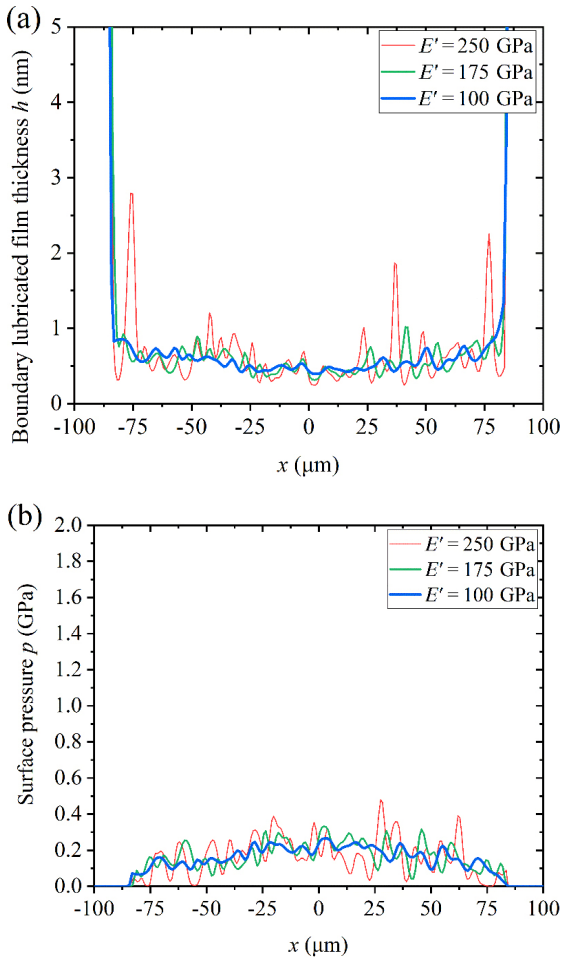

Fig. 12 Effect of effective elastic modulus on (a) boundary lubricated film thickness and (b) surface pressure.

based on a relatively low elastic modulus.

The above results (the effects of contact surface, surface roughness, and material elastic modulus on the film thickness and surface pressure of water-based boundary lubrication) indicate that the water-based liquid lubrication mechanism resulted in an ultralow friction during running-in combined with relevant experimental literatures [22, 31, 32]. Prior to running-in, the contact pressure is relatively high under the ball–disk contact. The water-based lubricant medium doesn't support the load to form a boundary lubricated film. The surface pressure is primarily generated by rough surface asperities in the lubricated contact area. During running-in, the contact area increases, while the contact pressure can be decreased. The surface pressures can be mainly supported by surface force effects, especially hydration effect. Hence, a thicker boundary lubrication film is obtained compared with that prior to running-in. Water molecules easily enters the contact area to form an effective lubricated water film. Simultaneously, a tribochemical reaction is occurred during running-in, and a new tribochemical reaction film is generated on the contact surface, e.g., the silicon dioxide reaction layer, thereby reducing the equivalent elastic modulus of the contact area. The new reaction layer can further reduce the pressure in the contact area. Based on the characteristics of hydration lubrication, the shearing force is extremely weak, which is beneficial for achieving ultralow friction lubrication and excellent lubrication performance. Therefore, to achieve water-based liquid superlubricity, the contact pressure should be within the carrying capacity of surface force effects (hydration effect and electric double layer).

4 Conclusions

A model for analyzing the water-based boundary lubricated contact based on surface force effects is proposed herein. The model enabled a deterministic analysis of the boundary lubricated contact behavior of smooth and rough surfaces. Based on the results and discussion, the following conclusions can be obtained:

1) Considering surface force effects, a water-based boundary lubricated contact mechanical model is established and can be used to deterministically analyze water-based boundary lubricated contact behaviors of different scales.

2) Under different gaps, the surface force interacting with the solid–liquid interfacial effect can result in different bearing load capabilities. Surface force interaction distribution is directly affected through regulating the hydration effect.

3) In the soft material ball contact on the smooth plane, the electric double layer and van der Waals force effects can be supported the relatively low normal load with a long contact gap, whereas the high normal load is supported by the hydration effect, and the contact gap is in the molecular scale.

4) The contact radius, surface roughness, and contact material properties significantly influence the boundary lubricated contact behavior based on the surface force effects. The contact area can be increased, whereas

the surface roughness and elastic modulus of the surface material are decreased during running-in; consequently, the contact pressure can be gradually decreased and boundary lubricated film can be formed at the same time. When the contact pressure is equivalent to the interaction range of the hydration surface force, a hydrated film can be formed in the entire contact area. According to the characteristics of the hydrated film, liquid superlubricity can be ultimately realized.

Acknowledgements

This study was financially supported by the National Natural Science Foundation of China (51922058) and Natural Science Foundation of Fujian Province (2021J05055).

References

[1] Ball P. Water as an active constituent in cell biology. *Chem Rev* **108**(1): 74–108 (2008)

[2] Seror J, Zhu L Y, Goldberg R, Day A J, Klein J. Supramolecular synergy in the boundary lubrication of synovial joints. *Nat Commun* **6**(1): 6497 (2015)

[3] Guo Z W, Yuan C Q, Liu A X, Jiang S. Study on tribological properties of novel biomimetic material for water-lubricated stern tube bearing. *Wear* **376–377**: 911–919 (2017)

[4] Mei D, Lin B, Sui T, Wang A, Shuai Y, Qiang Y. The excellent anti-wear and friction reduction properties of silica nanoparticles as ceramic water lubrication additives. *Ceram Int* **44**(12): 14901–14906 (2018)

[5] Wang Y R, Yu Q L, Cai M R, Shi L, Zhou F, Liu W M. Synergy of lithium salt and non-ionic surfactant for significantly improved tribological properties of water-based fluids. *Tribol Int* **113**: 58–64 (2017)

[6] Björneholm O, Hansen M H, Hodgson A, Liu L M, Bluhm H. Water at interfaces. *Chem Rev* **116**(13): 7698–7726 (2016)

[7] Chen L, Qian L M. Role of interfacial water in adhesion, friction, and wear—A critical review. *Friction* **9**(1): 1–28 (2021)

[8] Israelachvili J N. *Intermolecular and Surface Forces, 3rd Edition*. San Diego (USA): Elsevier Academic Press Inc., 2011.

[9] Funari R, Matsumoto A, de Bruyn J R, Shen A Q. Rheology of the electric double layer in electrolyte solutions. *Anal Chem* **92**(12): 8244–8253 (2020)

[10] Kelsall G H, Zhu Y, Spikes H A. Electrochemical effects on friction between metal oxide surfaces in aqueous solutions. *Faraday Trans* **89**(2): 267–272 (1993)

[11] Bo Z, Umehara N. Hydrodynamic lubrication theory considering electric double layer for very thin water film lubrication of ceramics. *JSME Int J Ser C* **41**(2): 285–290 (1998)

[12] Huang P, Wong P L, Meng Y G, Wen S Z. Influences of electric double layer on thin lubrication film thickness and pressure. (in Chinese). *Chin J Mech Eng* **38**(8): 9–13 (2002)

[13] Zuo Q Y, Huang P, Su F H. Theory analysis of asymmetrical electric double layer effects on thin film lubrication. *Tribol Int* **49**: 67–74 (2012)

[14] Xie G X, Guo D, Luo J B. Lubrication under charged conditions. *Tribol Int* **84**: 22–35 (2015)

[15] Fang Y F, Ma L R, Luo J B. Modelling for water-based liquid lubrication with ultra-low friction coefficient in rough surface point contact. *Tribol Int* **141**: 105901 (2020)

[16] Leikin S, Parsegian V A, Rau D C. Hydration forces. *Annu Rev Phys Chem* **44**(1): 369–395 (1993)

[17] Faraudo J, Bresme F. Origin of the short-range, strong repulsive force between ionic surfactant layers. *Phys Rev Lett* **94**(7): 077802.1–077802.4 (2005)

[18] Klein J. Hydration lubrication. *Friction* **1**(1): 1–23 (2013)

[19] Briscoe W H, Titmuss S, Tiberg F, Thomas R, Mcgillivray D, Klein J. Boundary lubrication under water. *Nature* **444**(7116): 191–194 (2006)

[20] Ma L R, Gaisinskaya-Kipnis A, Kampf N, Klein J. Origins of hydration lubrication. *Nat Commun* **6**: 6060 (2015)

[21] Diao Y J, Espinosa-Marzal R M. Molecular insight into the nanoconfined calcite–solution interface. *Proc Natl Acad Sci USA* **113**(43): 12047–12052 (2016)

[22] Li Y Z, Li S W, Bai P P, Jia W, Tian Y. Surface wettability effect on aqueous lubrication: Van der Waals and hydration force competition induced adhesive friction. *J Colloid Interface Sci* **599**: 667–675 (2021)

[23] Luo J B, Zhou X. Superlubricitive engineering—Future industry nearly getting rid of wear and frictional energy consumption. *Friction* **8**(4): 643–665 (2020)

[24] Luo J B, Liu M, Ma L R. Origin of friction and the new frictionless technology—Superlubricity: Advancements and future outlook. *Nano Energy* **86**: 10.6092 (2021)

[25] Li J J, Zhang C H, Deng M M, Luo J B. Investigations of the superlubricity of sapphire against ruby under phosphoric acid lubrication. *Friction* **2**(2): 164–172 (2014)

[26] Deng M M, Zhang C H, Li J J, Ma L R, Luo J B. Hydrodynamic effect on the superlubricity of phosphoric acid between ceramic and sapphire. *Friction* **2**(2): 173–181 (2014)

[27] Ge X Y, Halmans T, Li J J, Luo J B. Molecular behaviors in thin film lubrication—Part three: Superlubricity attained by polar and nonpolar molecules. *Friction* **7**(6): 625–636 (2019)

[28] Liang H, Guo D, Luo J B. Film forming behavior in thin film lubrication at high speeds. *Friction* **6**(2): 156–163 (2018)

[29] Zhang S H, Qiao Y J, Liu Y H, Ma L R, Luo J B. Molecular behaviors in thin film lubrication—Part one: Film formation for different polarities of molecules. *Friction* **7**(4): 372–387 (2019)

[30] Han T Y, Zhang C H, Luo J B. Macroscale superlubricity enabled by hydrated alkali metal ions. *Langmuir* **34**(38): 11281–11291 (2018)

[31] Han T Y, Zhang C H, Li J J, Yuan S H, Luo J B. Origins of superlubricity promoted by hydrated multivalent ions. *J Phys Chem Lett* **11**(1): 184–190 (2020)

[32] Li S W, Bai P P, Li Y Z, Jia W, Tian Y. Extreme-pressure superlubricity of polymer solution enhanced with hydrated salt ions. *Langmuir* **36**(24): 6765–6774 (2020)

[33] Chu L M, Lin J R, Chen J L. Effects of surface roughness and surface force on the thin film elastohydrodynamic lubrication of circular contacts. *Z Naturforsch A* **67**(6–7): 412–418 (2012)

[34] Zhang S W, Zhang C H, Hu Y Z, Ma L R. Numerical simulation of mixed lubrication considering surface forces. *Tribol Int* **140**: 105878 (2019)

[35] Muller V M, Yushchenko V S, Derjaguin B V. On the influence of molecular forces on the deformation of an elastic sphere and its sticking to a rigid plane. *J Colloid Interface Sci* **77**(1): 91–101 (1980)

[36] Yu N, Polycarpou A A. Adhesive contact based on the Lennard-Jones potential: A correction to the value of the equilibrium distance as used in the potential. *J Colloid Interface Sci* **278**(2): 428–435 (2004)

[37] Polonsky I A, Keer L M. A numerical method for solving rough contact problems based on the multi-level multi-summation and conjugate gradient techniques. *Wear* **231**(2): 206–219 (1999)

[38] Liu S B, Wang Q, Liu G. A versatile method of discrete convolution and FFT (DC-FFT) for contact analyses. *Wear* **243**(1–2): 101–111 (2000)

[39] Medina S, Dini D. A numerical model for the deterministic analysis of adhesive rough contacts down to the nano-scale. *Int J Solids Struct* **51**(14): 2620–2632 (2014)

[40] Bazrafshan M, de Rooij M B, Valefi M, Schipper D J. Numerical method for the adhesive normal contact analysis based on a Dugdale approximation. *Tribol Int* **112**: 117–128 (2017)

[41] Banquy X, Le Dévédec F, Cheng H, Faivre J, Zhu J X X, Valtiner M. Interaction forces between pegylated star-shaped polymers at mica surfaces. *ACS Appl Mater Interfaces* **9**(33): 28027–28033 (2017)

[42] Hu Y Z, Tonder K. Simulation of 3-D random rough surface by 2-D digital filter and Fourier analysis. *Int J Mach Tool Manuf* **32**(1–2): 83–90 (1992)

Yanfei FANG. He received his Ph.D. degree in mechanical engineering from South China University of Technology, Guangzhou, China in 2017. Following a postdoctoral period at the State Key Laboratory of Tribology of Tsinghua University, he is now working as a lecturer in the College of Mechanical Engineering and Automation, Huaqiao University in Xiamen, China. His research area is mainly about thin film lubrication and engineering tribology.

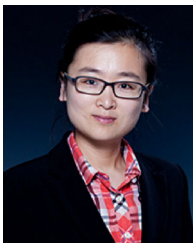

Liran MA. She received her bachelor degree from Tsinghua University in 2005, and received her Ph.D. degree from Tsinghua University in 2010. Following a postdoctoral period at the Weizmann Institute of Science in Israel, she is now working as an associate professor in State Key Laboratory of Tribology, Tsinghua University. Her current research interests are tribology and surface & interface science. She has published over 60 SCI papers. She was elected as the Young Chang Jiang Scholar in 2015.